C. R. Mecanique 345 (2017) 259–270

Contents lists available at ScienceDirect

Comptes Rendus Mecanique

www.sciencedirect.com

Two-phase flow patterns and size distribution of droplets in a microfluidic T-junction: Experimental observations in the squeezing regime

Yassine Mahdi [a,b,*], Kamel Daoud [a], Lounès Tadrist [b]

[a] University of Sciences and Technology Houari Boumediene, Faculty of Mechanical Engineering and Process Engineering, Laboratory of transfer phenomena, BP 32 Bab Ezzouar, 16111 Algiers, Algeria
[b] Aix-Marseille Université, Laboratoire IUSTI, CNRS UMR 7343, 13453 Marseille cedex 13, France

ARTICLE INFO

Article history:
Received 16 August 2016
Accepted 6 February 2017
Available online 21 February 2017

Keywords:
Microfluidics
Two-phase flow patterns
T-junction
Coefficient of variation
Size distribution

ABSTRACT

Generating micrometer sized droplets has been studied in a microfluidic system with T-junction geometry 250 µm in internal diameter and with PTFE capillary tubing. Several experiments were conducted by varying the flow rate of the dispersed phase from $2.78 \cdot 10^{-11}$ m^3/s to $5.28 \cdot 10^{-9}$ m^3/s and that of the continuous phase from $2.78 \cdot 10^{-10}$ m^3/s to $1.94 \cdot 10^{-9}$ m^3/s. The visualization of different flow regimes (drop, plug, and annular) was carried out for three configurations (not inverted in a horizontal position, inverted in a horizontal position, and inverted in a vertical position) for low capillary numbers. The model of Gauss was also chosen for a droplet size distribution in the dispersed phase, with the flow quality x varying from 0.016 to 0.44. The evolution of the drop size distribution as a function of the flow quality in the dispersed phase shows that the variation coefficient of the droplet's diameter is inversely proportional to the flow quality.

1. Introduction

Droplets are often encountered in multiphase microfluidics and have many potential applications in emulsions and are present in many everyday life products. They may be natural, as in the case of milk, egg yolk or the protective film on the skin or produced artificially for sauces, creams, gels, or paints. Therefore, they are of interest to the food, cosmetic or pharmaceutical industries and frequently found in many reactors and unit operations. The control and stability of these emulsions are primordial from a chemical engineering point of view. One of the most common techniques for their training is to emulsify a phase in another using a mechanical stirrer, a surfactant, and optionally a stabilizer. Thus, the dispersed phase droplets in the order of tens nanometers to a few hundred microns are generated in a continuous phase. A wide distribution of particles is obtained mainly due to the coalescence of the drops within the production vessel [1–4].

Therefore, the development of a device to control the generation of emulsions represents a major challenge for the development of water in an oil emulsion or of oil in water.

* Corresponding author at: University of Sciences and Technology Houari Boumediene, Faculty of Mechanical Engineering and Process Engineering, Laboratory of transfer phenomena, BP 32 Bab Ezzouar, 16111 Algiers, Algeria.
E-mail addresses: ymahdi@usthb.dz, mahdi.e@hotmail.fr (Y. Mahdi).

http://dx.doi.org/10.1016/j.crme.2017.02.001
1631-0721/

Nomenclature

Ca	Capillary number, ($Ca = \frac{\mu U}{\gamma}$)	U_c	Superficial velocity of the continuous phase ..... $m{\cdot}s^{-1}$
CV	Coefficient of variation	U_d	Superficial velocity of the dispersed phase ..... $m{\cdot}s^{-1}$
D	Capillary tube diameter ..... m	V_d	Volume of droplet ..... m^3
F	Frequency ..... s^{-1}	x	Dispersed phase flow quality $x = (\frac{\dot{m}_d}{\dot{m}_d+\dot{m}_c})$
G	Gravity acceleration ..... $m{\cdot}s^{-2}$	*Greek letters*	
L_c	Capillary length ..... m	$\alpha, \beta, \varepsilon$	Fitting parameters
d_d	Droplet diameter ..... m	γ	Interfacial tension ..... $N{\cdot}m^{-1}$
$\dot{m}_c$	Mass flow rate of the continuous phase ..... $kg{\cdot}s^{-1}$	σ	Surface tension ..... $N{\cdot}m^{-1}$
$\dot{m}_d$	Mass flow rate of the dispersed phase $kg{\cdot}s^{-1}$	μ	Dynamic viscosity ..... Pa·s
n	Number of samples	ρ_c	Density of the continuous phase ..... $kg{\cdot}m^{-3}$
Q_c	Volumetric flow rates of the continuous phase ..... $m^3{\cdot}s^{-1}$	ρ_d	Density of the dispersed phase ..... $kg{\cdot}m^{-3}$
Q_d	Volumetric flow rate of the dispersed phase ..... $m^3{\cdot}s^{-1}$	*Subscripts*	
Re_c	Reynolds number of the continuous phase, ($Re_c = \frac{\rho_c U_c D}{\mu_c}$)	C	Continuous phase (oil)
Re_d	Reynolds number of the dispersed phase, ($Re_d = \frac{\rho_d U_d D}{\mu_d}$)	D	Dispersed phase (water)

The development of microfluidic systems that produce micro- and nano-drops inside microfluidic devices has received significant attention over the past five years.

Miniaturization in microfluidics allows the handling of small sample volumes. Reducing the size of the systems and of the samples will have more impact on the properties of the solutions and the rate of chemical reactions. This is partly due to the fact that when the size of the devices and of the samples decreases, the surface-to-volume ratio increases [1].

Many investigators exhibited an interest in the production mechanism of the drops using T-junction microfluidic devices and critical process parameters [5–17].

Kabayashi [18], Wacker [19], and Husney [20] determined the influence of viscosity in a two-phase system. Husney [20] studied the formation of drops and the dynamics of Newtonian and non-Newtonian fluids by varying the viscosity of the two phases. They determined that the size of the drop is inversely proportional to the viscosity ratio.

Ismagilov [21] characterized a simple method for the formation of plugs with several reagents. For optimum mixing of the reactants in the micro-channels, the plugs with an initial distribution of the reactants can be formed simply by adjusting the phases of the flow.

Depending on the value of the capillary number (Table 1), three regimes can be observed, which are squeezing, dripping, and jetting regime [14,16,12,13,22].

In the squeezing regime, the capillary number is very small ($Ca < 10^{-2}$), the shear force exerted by the continuous phase is not enough to produce a detachment of the drop. The formation of the drop is controlled by the flow rate of the two phases [14].

The dripping regime is observed at high values of the capillary number ($Ca > 10^{-2}$), where the viscous forces are dominant compared to surface forces. Drops were formed at the intersection of two phases [12].

In the jetting regime, the flow is in jet form; in this case the generated droplets are smaller than the channel diameter. A filament of the dispersed phase is created and the generation of drops takes place farther than the intersection of two phases [23].

There is also some very interesting research work done on the generation of drops as well as the modeling of droplet size in microfluidic T-junctions using the squeezing regime. Garstecki et al. [14] have determined that the generation of drops at low capillary number in a *T-junction* is governed by the ratio of the flow rate of the two phases. They proposed the following model:

$$L/W = 1 + \alpha(Q_d/Q_c) \tag{1}$$

where L represents the drop length, W the channel width and α is a constant that depends on geometry. This model is valid for capillary numbers lower than 0.01.

Xu [9] and Fu [13] also studied the formation of drops in squeezing regime and proposed models that approximate that of Garstecki [14]: $L/W = 1.38 + 2.52\,Q_d/Q_c$ for Xu [9] and $L/W = 0.64 + 0.32\,Q_d/Q_c$ for Fu [13].

The present work aims to contribute to a better understanding of the two-phase flow of two immiscible liquids in a T-junction-shaped microfluidic system.

In the first part of this work, we describe the experimental set-up used to study the two-phase flow in the microfluidic system with different orientations of the T-junction and the method used for deducing the diameter of the drops followed

Table 1
Dimensionless numbers for the characterization of the two-phase flow.

Dimensionless number	Formula	Definition
Capillary number of the continuous phase	$Ca_c = \frac{\mu U_c}{\gamma}$	$\frac{\text{Viscous forces}}{\text{Interfacial forces}}$
Capillary number of the dispersed phase	$Ca_d = \frac{\mu U_d}{\gamma}$	$\frac{\text{Viscous forces}}{\text{Interfacial forces}}$
Reynolds number of dispersed phase	$Re_d = \frac{\rho_d U_d D}{\mu_d}$	$\frac{\text{Inertial forces}}{\text{Viscous forces}}$
Reynolds number of continuous phase	$Re_c = \frac{\rho_c U_c D}{\mu_c}$	$\frac{\text{Inertial forces}}{\text{Viscous forces}}$

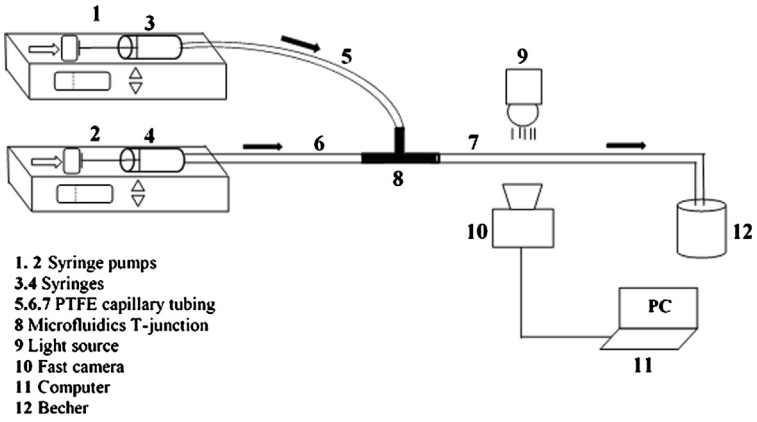

Fig. 1. Schematic of the experimental set-up.

by the results obtained in the visualization of the different flows regimes (annular, plug and drop) for each orientation of the T-junction.

A comparison between two usual models (Gauss and Lorentz) for the droplet size distribution was carried out. One model was finally chosen to monitor the distribution of the drops.

Finally, the evolution of the size distribution of the droplet diameter and the variation coefficient for each experiment were calculated. The limit between the polydispersity and the monodispersity of the droplets was determined as a function of the dispersed phase flow quality x.

2. Materials and methods

The schematic diagram of the experimental set-up for the study of a two-phase flow in a microfluidic system is shown in Fig. 1. The set-up consists of three main parts: the supply and control of the two phases (continuous and dispersed), the mixing zone and a last part for the visualization of flows. Two syringe pumps (Fresenius Vial, France) have been used to ensure the two phases fluids supply and the flow rate control with a precision of $\pm 0.2\%$ to $\pm 2\%$ depending on the flow rate ($2.78 \cdot 10^{-11}$–$2.78 \cdot 10^{-8}$ m^3/s). In the T-junction (Fig. 2) made of PTFE (Vici, France), the two fluids are supplied perpendicularly to one another in the junction, which is 250 µm in internal diameter. Capillary tubing made of PTFE (Kinesis, UK), 500 µm in internal diameter, insures the fluid transport of the two phases between the syringe and the T-junction.

The flow visualization is carried out using a high speed camera (FASTCAM, Photron Ultima 1024) with a macro lens of 105 mm (SIGMA, Japan) enabling the making of fast videos in 1024 by 512 at a rate of 1000 images per second. A cold-light source lamp (Dedolight 400D, Germany) is used as a light source in the visualization zone.

Distilled water and Vaseline oil were used for all experiments, and the properties of the two fluids are given in Table 2. The surface tension of the two fluids was measured with a tension meter (Kruss K20, Germany), the contact angle is measured by the sessile drop method at 23 °C, the viscosity of the two fluids is measured using a digital viscometer (Brookfield DV-E, USA), the density with a pycnometer, the refractive index of the fluids with an Abbe refractometer (Carl Zeiss) and that of the tube is given by the manufacturer's data sheet.

It is noted that the water contact angle is greater than 90°, which promotes the formation of water droplets in the oil, as Vaseline oil wets well the walls of the capillary tube with a lower contact angle of 90° (Table 2).

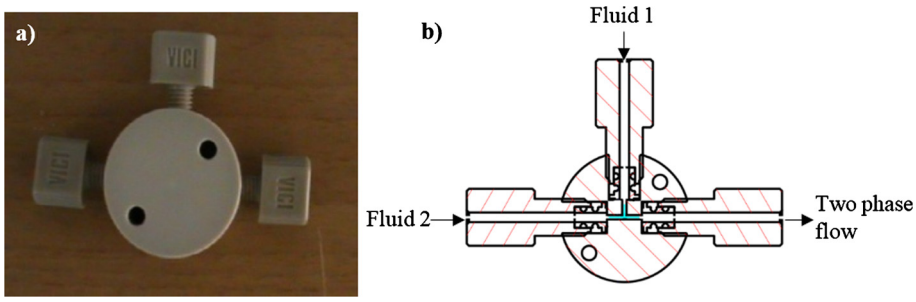

Fig. 2. (a) Photo and (b) scheme of the T- junction.

Table 2
Properties of the test fluids and PTFE tube and their precisions are given in the following table.

Properties	Distilled water	Vaseline oil	PTFE tube
Contact angle in a PTFE flat plate ($\theta°$)	109.78 ± 3	71.97 ± 3	–
Surface tension σ (mN/m)	$71.22 \pm 1\%$	$33.37 \pm 1\%$	–
Viscosity (Pa·s)	$8.9 \cdot 10^{-4} \pm 1\%$	$0.07 \pm 1\%$	–
Density ρ (kg/m^3)	$1006 \pm 0.2\%$	$850 \pm 0.2\%$	–
Refractive index [–]	1.33 ± 0.01	1.476 ± 0.01	1.350 ± 0.001

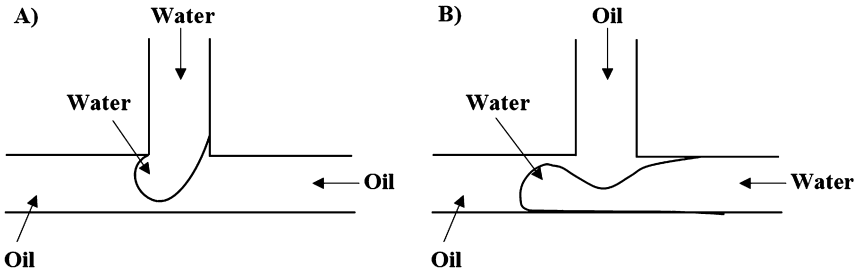

Fig. 3. Drop formation mechanism: a) in the orientation “a” and b) in the orientations “b” and “c” [9].

3. Results and discussion

3.1. Drops diameter and drop size distribution

The process of the video recordings and image captures are performed by the Photron FastCam Viewer Software. The process of images is performed with ImageJ software. The mean diameter and drop size distribution is obtained by measuring individually 150 drops to ensure a good sampling method. In order to evaluate the drop size distribution, a coefficient of variation (CV) is calculated using the following formula:

$$CV(\%) = (\sigma / \overline{L_d}) \times 100 \tag{2}$$

where $\sigma^2 = \sum_{i=1}^{n} \frac{(L_i - \overline{L_d})^2}{n-1}$ is the standard deviation of the droplet length and $\overline{L_d}$ the mean of the droplet length.

3.2. Visualization of the different flowing regimes

For the orientation “a” (Fig. 3a), the dispersed phase enters the main channel containing the continuous phase (oil) and then begins to undergo shear. A constriction is formed and more the dispersed (aqueous) phase moves in the main channel, more the constriction narrows until it intersects and forms a drop or a plug, and the process starts again [14].

For the orientations “b” and “c” (Fig. 3b), the dispersed phase (water) arrives in the main canal. Then, the continuous phase (oil) introduces vertically in the main canal and induces the development of a thread neck in the dispersed phase (water). Finally, the water thread collapses and breaks rapidly, forms a drop or a plug, and the process starts again [9].

Three regimes have been visualized at a low capillary number: namely annular, plug and drop regime. The capillary number is calculated using the superficial velocity and viscosity of the continuous phase [12,14,24,25].

In the annular regime, the initial dispersed phase (water) flows to the center of the capillary tube, whereas the initial continuous phase (oil) flows to a thin film between the dispersed phase fluid and the capillary tube wall.

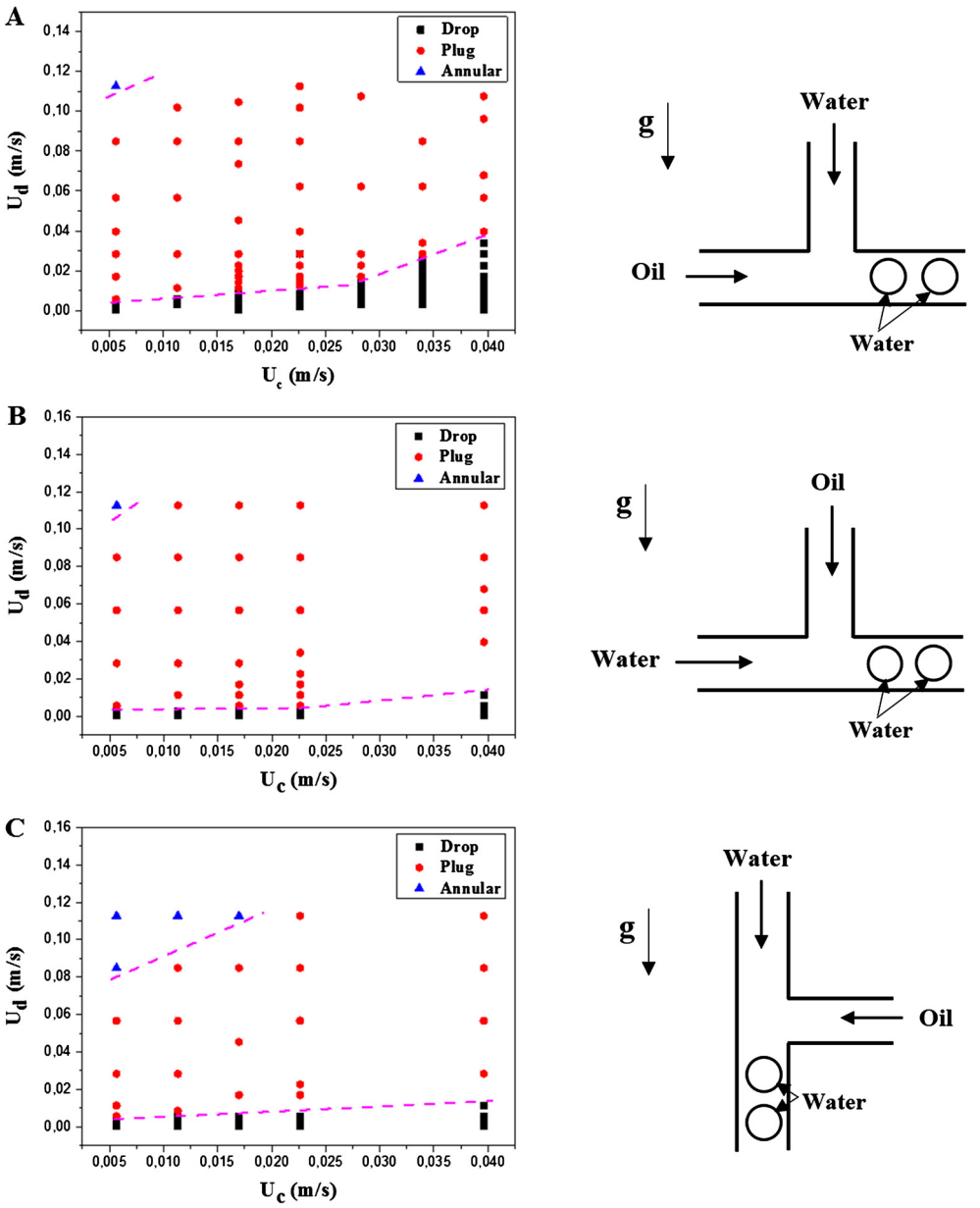

Fig. 4. Two-phase flow patterns for each orientation of the T-junction. a) Flow map of the two-phase flow in the horizontal position of the T-junction, b) Flow map of the two phases flow in the horizontal position of the T-junction and inversion of the fluids, c) Flow map in the vertical position and with inversion of the fluids.

The annular flow (Fig. 5) occurs for high speeds of the dispersed phase (water). In the configuration where the T-junction is in a horizontal position and with non-inversed fluids, the annular regime is observed for a continuous phase flow rate (oil) of $2.8 \cdot 10^{-10}$ m^3/s and a dispersed phase flow rate (water) of $5.5 \cdot 10^{-7}$ m^3/s; for the inversed configuration in a vertical position, a dispersed phase flow rate ranges from $4.2 \cdot 10^{-7}$ to $5.5 \cdot 10^{-7}$ m^3/s and from $2.8 \cdot 10^{-10}$ to $1.1 \cdot 10^{-7}$ m^3/s for the continuous phase. The superficial velocity and the Reynolds number of the continuous phase (oil) varies between $U_c = 5.7 \cdot 10^{-3}$ m/s, $Re_{oil} = 3 \cdot 10^{-2}$ to $U_c = 2.3 \cdot 10^{-2}$ m/s, $Re_{oil} = 0.145$. The superficial velocity and the Reynolds number of the dispersed phase (water) vary between $U_d = 8.5 \cdot 10^{-2}$ m/s, $Re_{water} = 49$ to $U_d = 0.113$ m/s, $Re_{water} = 64$.

In the plug flow regime (Fig. 6), the dispersed phase forms a plug with an equivalent diameter bigger than the channel diameter. The plugs are separated by slugs of the continuous phase, where probably a thin layer of the continuous phase flows between the plug and the wall of the capillary tube. As we can see in Fig. 4, the plug flowing occupies a big surface ranging, for the non-inverted configuration in the horizontal position, from $U_c = 5.6 \cdot 10^{-3}$ m/s, $Re_{oil} = 3.6 \cdot 10^{-2}$ to $U_c =$

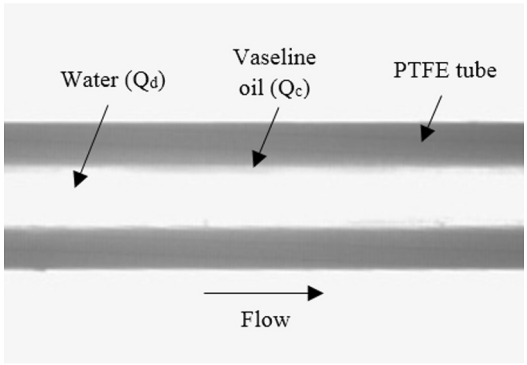

Fig. 5. Annular flow in the configuration "a": $U_c = 2.8 \cdot 10^{-4}$ m/s (oil) and $U_d = 5.5 \cdot 10^{-3}$ m/s (water).

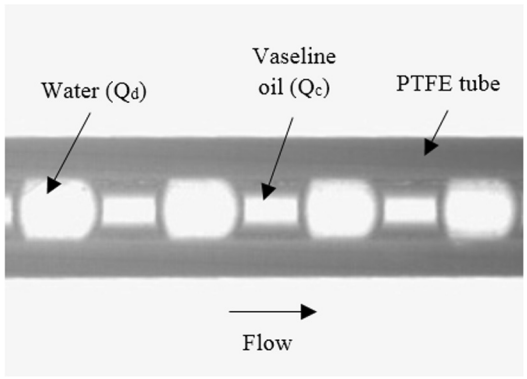

Fig. 6. Plug flow in the configuration "a" $U_c = 2.3 \cdot 10^{-2}$ m/s (oil) and $U_d = 0.11$ m/s (water).

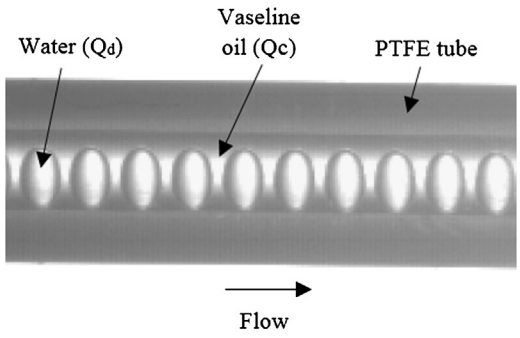

Fig. 7. Drop flow in the configuration "a": $U_c = 4 \cdot 10^{-2}$ m/s (oil) and $U_d = 5.6 \cdot 10^{-3}$ m/s (water).

$4 \cdot 10^{-2}$ m/s, $Re_{oil} = 0.25$ for the continuous phase (oil) and from $U_d = 5.65 \cdot 10^{-3}$ m/s, $Re_{water} = 3$ to $U_d = 0.11$ m/s, $Re_{water} = 60$ for the dispersed phase (aqueous).

The flow pattern of the drop regime (Fig. 7) is observed when the dispersed phase forms spherical drops with diameters smaller than the internal capillary tube diameter. The drop regime is observed at superficial velocities and Reynolds number in the non-inversed configuration (a) in the horizontal position ranging from $U_c = 5.6 \cdot 10^{-3}$ m/s, $Re_{oil} = 4 \cdot 10^{-2}$ to $U_c = 4 \cdot 10^{-2}$ m/s, $Re_{oil} = 0.25$ for the continuous phase (oil) and from $U_d = 6 \cdot 10^{-4}$ m/s, $Re_{water} = 0.32$ to $U_d = 3.4 \cdot 10^{-2}$ m/s, $Re_{water} = 19$ for the dispersed phase (water).

3.3. Measurement of the drop diameter

The diameter of the drops (water) is measured in the capillary tube just at the end of the T-junction. For each experience and in order to obtain good sampling, 150 images were processed. A number distribution is obtained and the average

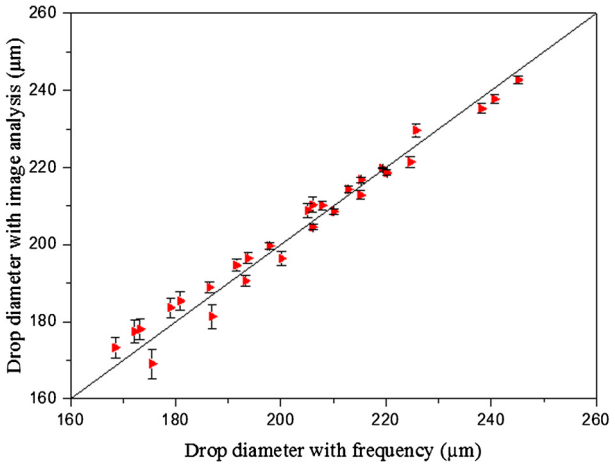

Fig. 8. Droplet diameter with image analysis vs. drop diameter with frequency equation.

diameter is calculated using the following formula:

$$d_{\mathrm{d}} = \frac{\sum d_i n_i}{\sum n_i} \tag{3}$$

where n_i is the number of droplets with diameter d_i.

The observed drops are not spherical in shape due to a deformation in the radial direction. This deformation is due to the capillary tube curvature [26–29]. In order to prove that the deformation occurs only in the radial direction and validate the method with image processing, a comparison of lengths is realized by the frequency method.

The drop generation frequency can be expressed by the following equation:

$$f = \frac{Q_{\mathrm{d}}}{V_{\mathrm{d}}} \tag{4}$$

with Q_{d} the dispersed phase flow and V_{d} the drop volume.

The capillary drop length is $L_{\mathrm{c}} = \sqrt{\frac{\gamma}{\Delta\rho g}} = 6.38$ mm with γ the interfacial tension between the water and the oil, $\Delta\rho$ the density difference and g the gravitational acceleration. This length ($L_{\mathrm{c}} = 6.38$ mm) is great compared to the drop length, whose values are smaller than the capillary tube diameter ($d_{\mathrm{c}} = 0.5$ mm); it means that the predominant capillary forces and gravitational forces can be neglected. Hence, the drop will have a spherical shape and a volume is (equation (5)):

$$V_{\mathrm{d}} = \frac{1}{6}\pi d^3 \tag{5}$$

By replacing it in the frequency equation, it gives (equation (6)):

$$d = \sqrt[3]{\frac{6Q_{\mathrm{d}}}{\pi f}} \tag{6}$$

This formula is used in order to determine drop diameters, to validate the method, and to demonstrate that drop deformation occurs only in the radial direction.

Fig. 8 shows a good dispersion around the line $y = x$ and shows that the diameters obtained by image analysis are almost the same values obtained by the frequency except for small diameters where the droplets have polydispersity; the frequency equation does not give a precise value where the distribution is wide. Size distribution of droplet diameter will be treated later on in this paper.

If the drops present monodispersity, measurements using frequencies gives good results. If the drops are polydisperse in size, measurements using frequencies are not accurate because the drops do not have the same diameter. However, the imaging measurement takes into account the diameter of each drop by calculating the weighted mean of the size distribution obtained; with a good sampling (150 images for each diameter) the measurement error is very small (<6%).

Fig. 9 shows the evolution of the mean diameter obtained by imaging as a function of the flow ratio of the two phases.

We notice that the length of the drops is proportional to the two-phase flow ratio. This evolution of the drops length confirms the study of Garstecki [14] on the formation of low capillary number drops by showing that it depends only on the pressure forces exerted by the two fluids (dispersed and continuous); the evolution of size follows the following

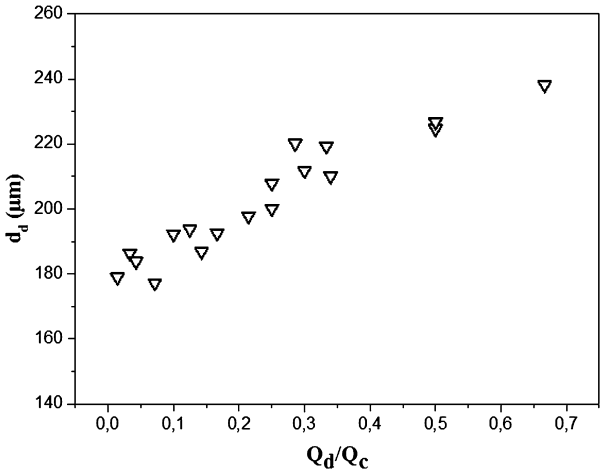

Fig. 9. Droplet diameter vs. two-phase flow ratio.

model:

$$L/w = 1 + \alpha(Q_d/Q_c) \tag{1}$$

This study follows the work of Xu [12], who gave a more general model than Garstecki [14]:

$$L/w = \varepsilon + \beta(Q_d/Q_c) \tag{7}$$

with L the length of the droplet, w the width of the microchannel, Q_c and Q_d the flow rate of the two phases (dispersed and continuous), ε and β are parameters than depend on the geometry of the T-junction.

According to Garstecki [14], the formation of a drop phenomenon in a T-junction at low capillary number can be explained as follows: the dispersed phase enters the main channel containing the continuous phase (oil in this case) and then begins to undergo shear. A constriction is formed and the more the dispersed (aqueous) phase advances in the main channel, the more constriction narrows until it intersects and forms a drop.

In order to follow the evolution of the droplet size distribution for each experiment, the number distribution was represented with a sampling of 150 values (which corresponds to 150 images). For each experiment and after testing several models, the better distribution is the Lorentz model (Eq. (8)):

$$f(d_d) = \frac{2A}{\pi}\frac{w}{4(d_d - \overline{d_d})^2 + w^2} \tag{8}$$

with $\overline{d_d}$, the mode or the median and w the full width at half maximum of the distribution.

The Lorentz model, even though it applies well to the distribution, was not chosen because, according to the definition, it model admits neither mean nor standard deviation. It makes it impossible to compare the average value calculated with formula (1) with that given by the model.

The model that has been chosen is Gauss' one (Eq. (9)). This model does not apply as well as that of Lorentz, but gives R^2 values close to 1 (Fig. 10 and Fig. 11).

$$f(d_d) = \frac{1}{\sigma\sqrt{2\pi}} e^{-\frac{1}{2}\left(\frac{d_d - \overline{d_d}}{\sigma}\right)^2} \tag{9}$$

with $\overline{d_d}$ the mean and σ^2 the variance. $\sigma^2 = \sum_{i=1}^{n} \frac{(d_d - \overline{d_d})^2}{n-1}$.

Gauss' law depends on two parameters, which are the mean μ and the standard deviation σ. These two parameters will help us to compare the mean given by the model and the one calculated with formula (1), and also to monitor the evolution of the distribution with a coefficient of variation which is the reported standard deviation to the mean.

Fig. 12 shows the mean diameter calculated with Eq. (3) as a function of the mean diameter given by the Gauss model. We note that the points are distributed around the straight line $y = 0.976x + 4.734$ and which approaches the axis $y = x$, which is why the average values given by the Gauss model approach those obtained by Eq. (3).

3.4. Evolution of the droplet size distribution

The variability of the data can often be best described as a relative change rather than as an absolute change, such as that shown by the standard deviation. A common way to express the variability that reflects its relative importance is the standard deviation relative to the mean diameter. This ratio, often expressed as a percentage, is called the coefficient of

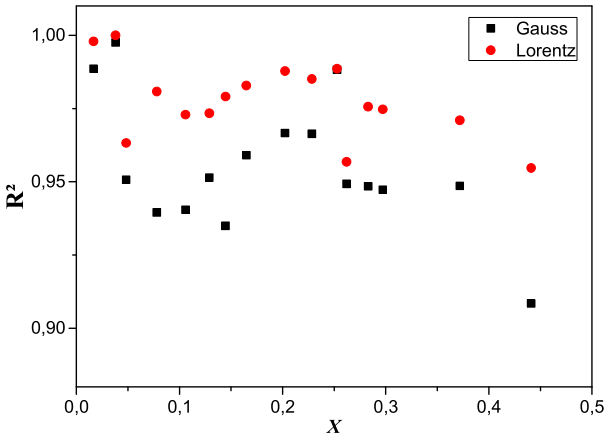

Fig. 10. Coefficient of determination vs. dispersed phase flow quality.

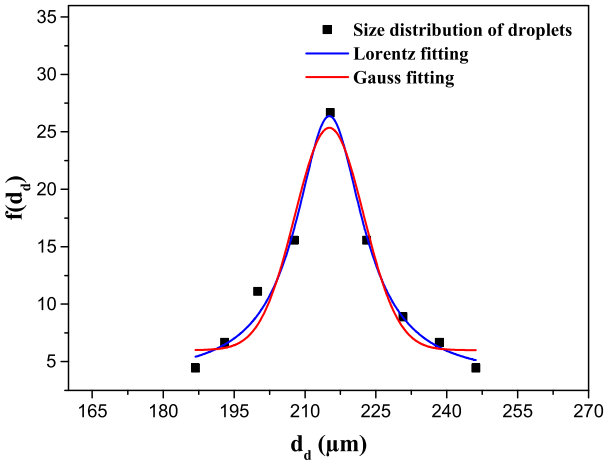

Fig. 11. Size distribution of droplets.

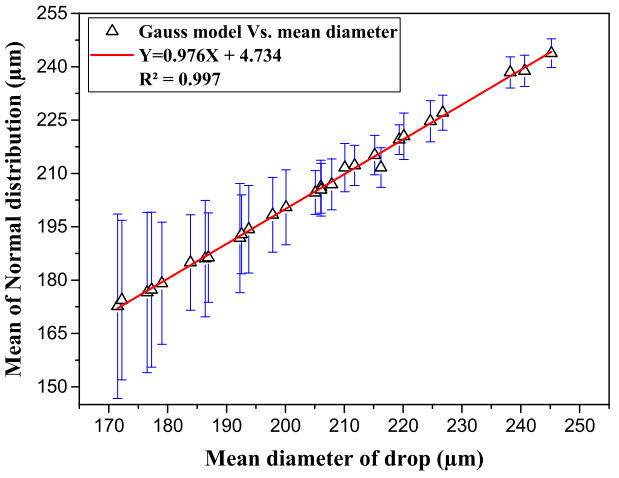

Fig. 12. Mean diameter given by the Gauss model as a function of the mean diameter calculated with Eq. (3).

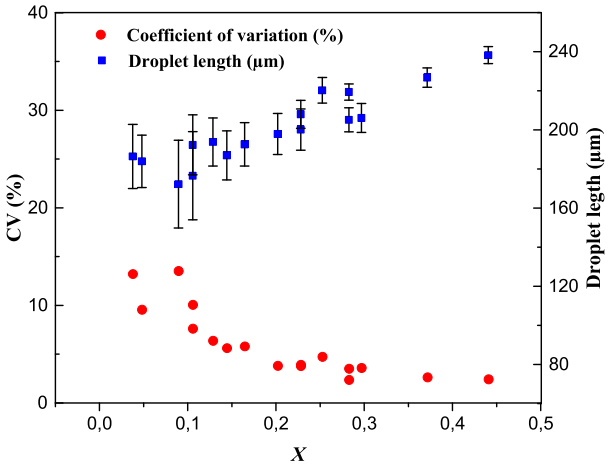

Fig. 13. Evolution of variation coefficient *CV* versus dispersed phase flow quality for the orientation case "a".

variation, abbreviated as *CV*. This way of expressing the variability is useful in many situations. It puts the variability in perspective relative to the magnitude of the measurements and allows a comparison of the variability of different kinds of measurements [30]. In the case of this study, it gives us the variability of the mean diameter, allowing us to determine the degree of monodispersity of the droplets.

It is well known that microfluidic systems generate monodisperse drops with $CV < 5\%$ [23]. Nevertheless, this is not always the case. That is why we studied the evolution of the coefficient of variation of the drops diameter throughout the drop regime.

Fig. 12 shows the evolution of the coefficient of variation as a function of the flow rate fraction of the dispersed phase to the non-inverted configuration. We notice at first glance that the variation coefficient is inversely proportional to the diameter of the drops. The more the diameter of the drops increases, the more *CV* decreases.

For low values of the dispersed phase flow quality, we notice that there is a polydispersity in the distribution with *CV* ranging from 14% to 5% for a flow quality less than 0.1. This can be seen in Fig. 13. This polydispersity is obtained for drop diameters ranging from 160 µm to 190 µm (Fig. 14).

For values of the dispersed phase flow quality greater than 0.1, we notice that there is a monodispersity in the distribution with a variation coefficient ranging from 5% to 1.6%, as shown in Fig. 13. This monodispersity is observed for diameters ranging from 195 µm to 240 µm (Fig. 14).

The drops begin having the same diameter when the flow quality of the dispersed phase increases while remaining in the drop regime flow, which results in an increased flow rate of the dispersed phase (aqueous in this case) and an increase in the drops size.

On flows mappings, we see that the points where flow quality is important are located in the area near the plug regime (close to the drop-plug transition zone) and an increase in speed of the two phases results in an increase in the diameter of the drops; the coefficient of variation decreases.

In Fig. 4, we see that the drop regime takes a large area on the flow map for the orientation "a" of the T-junction compared to the configurations "b" and "c", so that for the same superficial velocities of the dispersed and continuous phases, a drop regime is obtained in the orientation "a" and a plug regime in the orientations "b" and "c" of a T-junction.

The orientation of the T-junction that has a large area of drop regime in the two-phase flow pattern with low coefficients of variation is the orientation "a".

4. Conclusion

In the present work, an experimental setup involving a microfluidic T-junction, 250 µm in internal diameter, was made.

The visualization of the two-phase flow was performed at the capillary tube using a high-speed camera just at the exit of the T-junction. The three flow regimes (drop, plug, and annular) were observed, and mappings were plotted for the three configurations (not inverted in a horizontal position, inverted in a horizontal position and inverted in a vertical position). Each regime has been identified in relation to the two phase flows.

The diameter of the drops was calculated with a sampling of 150 images. A size distribution of each experiment was performed and modeled with Gauss' law. The coefficient of variation of each experiment was calculated to monitor the distribution. It was shown that the variation coefficient is inversely proportional to the flow quality of the dispersed phase. We were able to identify areas where the distribution presents a monodisperse drop size (<2%). The orientation of the T-junction that has a large area in the two-phase flow pattern with low coefficients of variation is the orientation "a". The

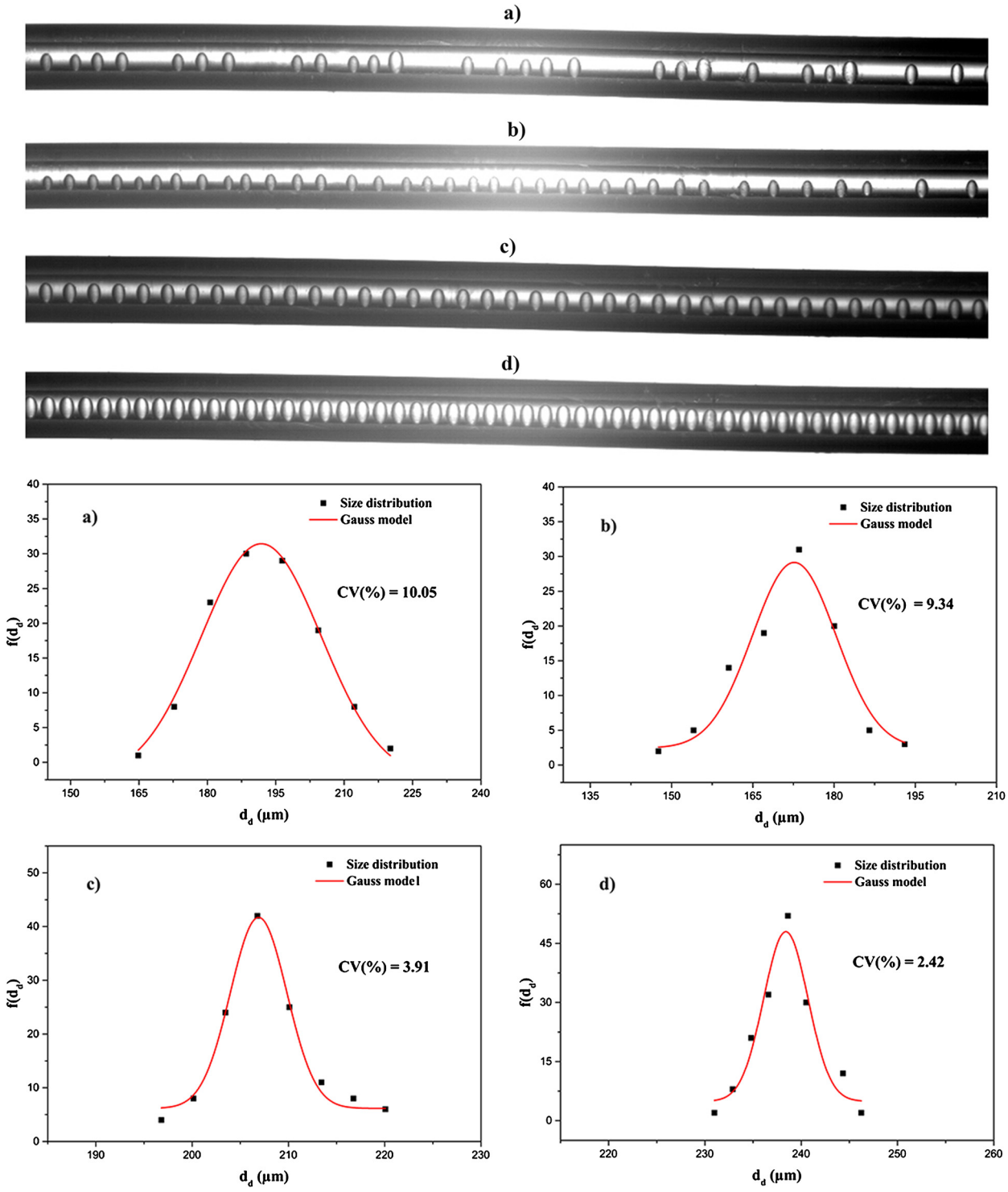

Fig. 14. Evolution of the drop size distribution function for the different orientations of the T-junction "a". The degree of the monodispersity is increased by increasing the quality of the dispersed phase flow. a) $U_c = 1.7 \cdot 10^{-2}$ m/s and $U_d = 1.7 \cdot 10^{-3}$ m/s, b) $U_c = 2.8 \cdot 10^{-2}$ m/s and $U_d = 5.6 \cdot 10^{-3}$ m/s, c) $U_c = 3.4 \cdot 10^{-2}$ m/s and $U_d = 8.5 \cdot 10^{-3}$ m/s, d) $U_c = 3.4 \cdot 10^{-2}$ m/s and $U_d = 2.2 \cdot 10^{-2}$ m/s.

observation of the two-phase flow patterns reveal that the dispersed phase is water (Q_d) and the continuous phase is oil (Q_c), regardless of the T-junction's orientation, and that the change is in the drop formation mechanism.

References

[1] C.N. Baroud, F. Gallaire, R. Dangla, Dynamics of microfluidic droplets, Lab Chip 10 (16) (2010) 2032–2045, http://dx.doi.org/10.1039/c001191f.
[2] D. Mark, S. Haeberle, G. Roth, F. von Stetten, R. Zengerle, Microfluidic lab-on-a-chip platforms: requirements, characteristics and applications, Chem. Soc. Rev. 39 (2010) 1153–1182, http://dx.doi.org/10.1039/B820557B.
[3] T.M. Squires, S.R. Quake, Microfluidics: fluid physics at the nanoliter scale, Rev. Mod. Phys. 77 (2005) 977–1026, http://dx.doi.org/10.1103/RevModPhys.77.977.
[4] G.M. Whitesides, The origins and the future of microfluidics, Nature 442 (2006) 368–373, http://dx.doi.org/10.1038/nature05058.
[5] I.Y. Chen, K.S. Yang, C.C. Wang, An empirical correlation for two-phase frictional performance in small diameter tubes, Int. J. Heat Mass Transf. 45 (17) (2002) 3667–3671, http://dx.doi.org/10.1016/S0017-9310(02)00074-1.
[6] H. Liu, Y. Zhang, Droplet formation in a T-shaped microfluidic junction, J. Appl. Phys. 106 (2009) 034906, http://dx.doi.org/10.1063/1.3187831.
[7] T. Glawdel, C. Elbuken, C.L. Ren, Droplet formation in microfluidic T-junction generators operating in the transitional regime. I. Experimental observations, Phys. Rev. E 85 (2012) 016322, http://dx.doi.org/10.1103/PhysRevE.85.016322.
[8] T. Glawdel, C. Elbuken, C.L. Ren, Droplet formation in microfluidic T-junction generators operating in the transitional regime. II. Modeling, Phys. Rev. E 85 (2012) 016323, http://dx.doi.org/10.1103/PhysRevE.85.016323.
[9] J.H. Xu, G.S. Luo, S.W. Li, G.G. Chen, Shear force induced monodisperse droplet formation in a microfluidic device by controlling wetting properties, Lab Chip 6 (1) (2005) 131–136, http://dx.doi.org/10.1039/b509939k.
[10] T. Thorsen, R. Roberts, F.H. Arnold, S.R. Quake, Dynamic pattern formation in a vesicle-generating microfluidic device, Phys. Rev. Lett. 86 (2001) 4163–4166, http://dx.doi.org/10.1103/PhysRevLett.86.4163.
[11] S. Yeom, S.Y. Lee, Dependence of micro-drop generation performance on dispenser geometry, Exp. Therm. Fluid Sci. 35 (8) (2011) 1565–1574, http://dx.doi.org/10.1016/j.expthermflusci.2011.07.008.
[12] J.H. Xu, S.W. Li, J. Tan, G.S. Luo, Correlations of droplet formation in T-junction microfluidic devices: from squeezing to dripping, Microfluid. Nanofluid. 5 (6) (2008) 711–717, http://dx.doi.org/10.1007/s10404-008-0306-4.
[13] T. Fu, Y. Ma, D. Funfschilling, H.Z. Li, Bubble formation and breakup mechanism in a microfluidic flow-focusing device, Chem. Eng. Sci. 64 (10) (2009) 2392–2400, http://dx.doi.org/10.1016/j.ces.2009.02.022.
[14] P. Garstecki, M.J. Fuerstman, H.A. Stonec, G.M. Whitesides, Formation of droplets and bubbles in a microfluidic T-junction scaling and mechanism of break-up, Lab Chip 6 (3) (2006) 437–446, http://dx.doi.org/10.1039/b510841a.
[15] G.F. Christopher, N.N. Noharuddin, J.A. Taylor, S.L. Anna, Experimental observations of the squeezing-to-dripping transition in T-shaped microfluidic junctions, Phys. Rev. E 78 (2008) 036317, http://dx.doi.org/10.1103/PhysRevE.78.036317.
[16] M.D. Menech, P. Garstecki, F. Jousse, H.A. Stone, Transition from squeezing to dripping in a microfluidic T-shaped junction, J. Fluid Mech. 595 (2008) 141–161, http://dx.doi.org/10.1017/S002211200700910X.
[17] V. Van Steijn, C.R. Kleijn, M.T. Kreutzer, Predictive model for the size of bubbles and droplets created in microfluidic T-junctions, Lab Chip 10 (19) (2010) 2513–2518, http://dx.doi.org/10.1039/c002625e.
[18] I. Kobayashi, S. Mukataka, M. Nakajima, Effects of type and physical properties of oil phase on oil in water emulsion droplet formation in straight through microchannel emulsification, experimental and CFD studies, Langmuir 21 (13) (2005) 5722–5730, http://dx.doi.org/10.1021/la050039n.
[19] J. Wacker, V.K. Parashar, M.A.M. Gijs, Influence of oil type and viscosity on droplet size in a flow focusing microfluidic device, Proc. Chem. 1 (1) (2009) 1083–1086, http://dx.doi.org/10.1016/j.proche.2009.07.270.
[20] H. Joeska, J.J. Cooper-White, The effect of elasticity on drop creation in T-shaped microchannels, J. Non-Newton. Fluid Mech. 137 (1–3) (2006) 121–136, http://dx.doi.org/10.1016/j.jnnfm.2006.03.007.
[21] L. Li, R.F. Ismagilov, Protein crystallization using microfluidic technologies based on valves droplets and slip chip, Annu. Rev. Biophys. 39 (2010) 139–158, http://dx.doi.org/10.1146/annurev.biophys.050708.133630.
[22] J. Sivasamy, T.N. Wong, N.T. Nguyen, L.T.H. Kao, An investigation on the mechanism of droplet formation in a microfluidic T-junction, Microfluid. Nanofluid. 11 (2011) 1–10, http://dx.doi.org/10.1007/s10404-011-0767-8.
[23] C.-X. Zhao, A.P.J. Middelberg, Two-phase microfluidic flows, Chem. Eng. Sci. 66 (7) (2011) 1394–1411, http://dx.doi.org/10.1016/j.ces.2010.08.038.
[24] S. Zhang, C. Guivier-Curien, S. Veesler, N. Candoni, Prediction of sizes and frequencies of nanoliter-sized droplets in cylindrical T-junction microfluidics, Chem. Eng. Sci. 138 (2015) 128–139, http://dx.doi.org/10.1016/j.ces.2015.07.046.
[25] M. Ildefonso, N. Candoni, S. Veesler, A. Cheap, Easy microfluidic crystallization device ensuring universal solvent compatibility, Org. Process Res. Dev. 16 (4) (2012) 556–560, http://dx.doi.org/10.1021/op200291z.
[26] S. Zeguai, S. Chikh, L. Tadrist, Experimental study of two-phase flow pattern evolution in a horizontal circular tube of small diameter in laminar flow conditions, Int. J. Multiph. Flow 55 (2013) 99–110, http://dx.doi.org/10.1016/j.ijmultiphaseflow.2013.04.008.
[27] Y. Han, N. Shikazono, Measurement of the liquid film thickness in micro tube slug flow, Int. J. Heat Fluid Flow 30 (5) (2009) 842–853, http://dx.doi.org/10.1016/j.ijheatfluidflow.2009.02.019.
[28] M. Mac Giolla Eain, V. Egan, J. Punch, Film thickness measurements in liquid–liquid slug flow regimes, Int. J. Heat Fluid Flow 44 (2013) 515–523, http://dx.doi.org/10.1016/j.ijheatfluidflow.2013.08.009.
[29] J.A. Howard, P.A. Walsh, Review and extensions to film thickness and relative bubble drift velocity prediction methods in laminar Taylor or slug flows, Int. J. Multiph. Flow 55 (2013) 32–42, http://dx.doi.org/10.1016/j.ijmultiphaseflow.2013.04.005.
[30] S. Bolton, C. Bon, Pharmaceutical Statistics, Practical and Clinical Applications, fifth edition, 2010, p. 16, Chapter I.